



ANNUAL REVIEWS **Further**

Click [here](#) to view this article's online features:

- Download figures as PPT slides
- Navigate linked references
- Download citations
- Explore related articles
- Search keywords

Elastocapillarity: Surface Tension and the Mechanics of Soft Solids

Robert W. Style,¹ Anand Jagota,² Chung-Yuen Hui,³
and Eric R. Dufresne⁴

¹Mathematical Institute, Oxford University, Oxford OX2 6GG, United Kingdom

²Department of Chemical and Biomolecular Engineering and Bioengineering Program, Lehigh University, Bethlehem, Pennsylvania 18015

³Department of Mechanical and Aerospace Engineering, Cornell University, Ithaca, New York 14850

⁴Department of Materials, ETH Zurich, CH-8093 Zurich, Switzerland;
email: eric.dufresne@mat.ethz.ch

Annu. Rev. Condens. Matter Phys. 2017. 8:99–118

First published online as a Review in Advance on
December 7, 2016

The *Annual Review of Condensed Matter Physics* is
online at conmatphys.annualreviews.org

<https://doi.org/10.1146/annurev-conmatphys-031016-025326>

Copyright © 2017 by Annual Reviews.
All rights reserved

Keywords

surface stress, capillarity, gels, elastomers, soft interfaces, analytical methods, numerical methods

Abstract

It is widely appreciated that surface tension can dominate the behavior of liquids at small scales. Solids also have surface stresses of a similar magnitude, but they are usually overlooked. However, recent work has shown that these can play a central role in the mechanics of soft solids such as gels. Here, we review this emerging field. We outline the theory of surface stresses, from both mechanical and thermodynamic perspectives, emphasizing the relationship between surface stress and surface energy. We describe a wide range of phenomena at interfaces and contact lines where surface stresses play an important role. We highlight how surface stresses cause dramatic departures from classic theories for wetting (Young–Dupré), adhesion (Johnson–Kendall–Roberts), and composites (Eshelby). A common thread is the importance of the ratio of surface stress to an elastic modulus, which defines a length scale below which surface stresses can dominate.

1. INTRODUCTION

Soft solids are ubiquitous. They include gels, creams, foams, rubbers, pressure-sensitive adhesives and much of biological tissue. Soft solids have long been incorporated in cosmetics, adhesives, sealants, and padding. Furthermore, exciting new applications are developing in surgery, tissue engineering, flexible electronics, and soft robotics (e.g., 1–8), often utilizing the fact that soft solids can exhibit mechanical phenomena that differ qualitatively from hard engineering materials (9). One key difference is that surface stresses, which play a minor role in the mechanics of stiff materials, can dominate the behavior of soft solids.

However, the importance of surface stresses on the mechanics of soft materials has only come to light in the past few years. For example, surface stresses stabilize the surface of a soft solid slab (10, 11) but break up soft solid filaments (12). Surface stresses resist the deformation of fluid inclusions in a soft solid and stiffen fluid–solid composites (13). Liquid droplets on soft substrates can violate the classic Young–Dupré equilibrium (14–16). Stiff solid particles adhered to soft substrates do not obey the standard models for adhesive contacts (17–19).

The surface of a material has an energy penalty per unit area of surface, the surface energy, γ (20). In liquids, the surface energy penalty gives rise to a tensile surface stress, Υ , that opposes surface stretching. It acts to minimize the surface-to-volume ratio of the liquid, causing liquid surfaces to be smooth and small droplets to bead up. Surface stress allows small dense objects to float at a liquid surface and is the source of the Laplace pressure difference across curved surfaces. Generally, Υ is a symmetric second-order, two-dimensional tensor. However, in simple liquids, Υ is isotropic and thus can be represented by a scalar Υ . Another convenient property of simple liquids is that $\gamma = \Upsilon$. This has led to γ and Υ being referred to interchangeably as the surface tension (20).

Surface energies and stresses in solids are different in two key ways from their liquid counterparts. First, the surface stress and surface energy are not generally equal, $\gamma \neq \Upsilon$, (21). Therefore, one must use the term surface tension carefully. Second, solid surface stresses can be anisotropic and even compressive (21–25).

The relative importance of surface stress and bulk elasticity is a matter of length scale. Just as a fluid’s surface tension creates a jump in hydrostatic pressure across a curved interface (the Young–Laplace equation), surface stress causes a jump in the stresses across a solid interface. For a solid surface with mean curvature \mathcal{K} and isotropic, uniform surface stress Υ , the jump in normal stress is simply $\Upsilon\mathcal{K}$. This stress jump drives local deformation in the bulk of the solid. For an elastic solid with Young’s modulus E , stresses balance so that $\Upsilon\mathcal{K} \sim \epsilon E$, where ϵ is the strain. Thus, we expect significant deformations ($\epsilon \sim 1$) when $1/\mathcal{K} \sim \Upsilon/E$. This defines an elastocapillary length, Υ/E . Generally, at scales much larger than Υ/E , surface effects are negligible. At scales much smaller than Υ/E , surface stresses dominate and one observes dramatic departures from classic behavior.

Elastocapillary phenomena at the continuum level are possible when Υ/E is much larger than molecular scales. The surface energies of soft materials are typically of order 10–100 mN/m (20). Thus elastocapillarity can be very important in soft polymeric materials like gels [$E \sim O(\text{kPa})$] and elastomers [$E \sim O(\text{MPa})$].

We briefly note that there is a large body of prior work that has focused on surface stresses in stiffer materials such as metals and other crystallographic solids (see previous reviews: 25–28). In this review, we focus on recent work that has evolved from new observations of surface stress effects in soft solids.

2. ELASTOCAPILLARY PHENOMENA AT INTERFACES

We begin this section by deriving the fundamental boundary condition balancing bulk and surface stresses across an interface—the equivalent of Laplace’s law for solids. Then, we discuss

the implications of this force balance in some examples involving two phases separated by an interface.

2.1. Surface Stress as a Boundary Condition at an Interface

The surface stress tensor, Υ , is the 2D analog of the more familiar 3D (Cauchy) stress tensor, σ . In 3D, the forces per unit area of a deformed surface (tractions) acting at a surface with normal \mathbf{n} are given by $\sigma \cdot \mathbf{n}$. The tractions can be resolved into a normal component, $\mathbf{n} \cdot \sigma \cdot \mathbf{n}$, and a shear component, $\mathbf{t} \cdot \sigma \cdot \mathbf{n}$, where \mathbf{t} is a unit vector tangential to the surface. Similarly, in 2D, the forces per unit length of a curve bounding a deformed surface with boundary normal \mathbf{b} are given by $\Upsilon \cdot \mathbf{b}$ (see **Figure 1**). Surface stresses always act in the plane of the surface and have a line-normal component, $\mathbf{b} \cdot \Upsilon \cdot \mathbf{b}$, and tangential component, $\mathbf{t} \cdot \Upsilon \cdot \mathbf{b}$, where \mathbf{t} is the vector tangent to the curve.

The essential physics of elastocapillary coupling lies in a connection between the surface stress and the bulk stress at the interface. The governing interfacial equation can be derived by considering the forces acting on the area of surface in **Figure 1**. The condition for static equilibrium is

$$\int_S \sigma_1 \cdot \mathbf{n} dS - \int_S \sigma_2 \cdot \mathbf{n} dS + \oint_C \Upsilon \cdot \mathbf{b} dl = 0. \quad (1)$$

Here, the integrals are in the deformed configuration and $\sigma_{1,2}$ are the true (Cauchy) stresses in the deformed body. Note that we have ignored any forces acting on the surface due to external potentials (e.g., surface charges in an electric field) and have assumed that the surface has no bending rigidity. The first two terms represent forces due to bulk stresses acting on either side of the area of interface, S . The last term is the contribution to total force due to surface stress. Using the surface divergence theorem, we can convert this term to a surface integral and then remove the integrals (as S is arbitrary) to obtain the generalization of Laplace's law:

$$(\sigma_1 - \sigma_2) \cdot \mathbf{n} = -\nabla^s \cdot \Upsilon, \quad (2)$$

where, ∇^s is the surface gradient operator (23, 24, 29). When the surface stress is isotropic, $\Upsilon = \gamma \mathbf{I}_2$, where \mathbf{I}_2 is the 2D identity tensor, this boundary condition simplifies to

$$(\sigma_1 - \sigma_2) \cdot \mathbf{n} = \gamma \mathcal{K} \mathbf{n} - \nabla^s \gamma, \quad (3)$$

where curvature $\mathcal{K} = \nabla^s \cdot \mathbf{n}$. Note that the stresses due to the first term on the right-hand side are always normal to the interface. The stresses due to the second term are always in-plane and equivalent to Marangoni stresses in a liquid (30). If the surface stress is both isotropic and uniform,

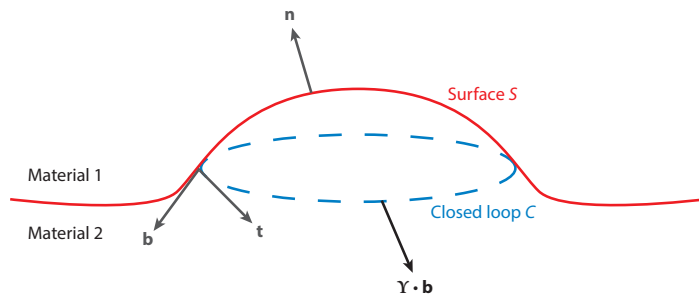


Figure 1

Schematic diagram for deriving the equation for force equilibrium at an interface.

$$\nabla^* \Upsilon = 0, \text{ and}$$

$$(\sigma_1 - \sigma_2) \cdot \mathbf{n} = \Upsilon \mathcal{K}, \quad (4)$$

which reduces to the Young–Laplace law for fluid interfaces ($\Delta P = \gamma \mathcal{K}$). The simplified boundary condition of Equation 4 shows excellent agreement with a wide range of experimental observations in hydrogels and silicone gels (e.g., 12, 13, 16, 19, 31–34). The implications for more complex surface stresses are just beginning to be explored (35).

2.2. Surface Stresses Flatten Slabs

The simplest manifestation of the competition between surface stress and elasticity is the smoothing of features on solid slabs (11, 33, 36, 37). An example of this is the change in shape of soft gels that are released from rigid, patterned molds. **Figure 2** (*inset*) shows the profile of a gel before and after release from a mold with a square wave pattern. Upon release, sharp corners are rounded out, and the overall amplitude of the pattern is reduced. Flattening is strong for softer gels and shorter wavelengths (**Figure 2**).

The flattening process is intimately linked to the elastocapillary length, Υ/E (11). Consider a simplified experiment with a solid having an initially sinusoidal surface profile of wavelength λ and amplitude A (11). According to Equation 4, the capillary stress normal to the surface is $\sigma_\Upsilon = \Upsilon \mathcal{K}$, where $\mathcal{K} \sim A/\lambda^2$ is the surface curvature. This stress drives flattening and is opposed by the elastic stress. Complete flattening requires the strain in the solid $\epsilon \sim A/\lambda$, so the elastic

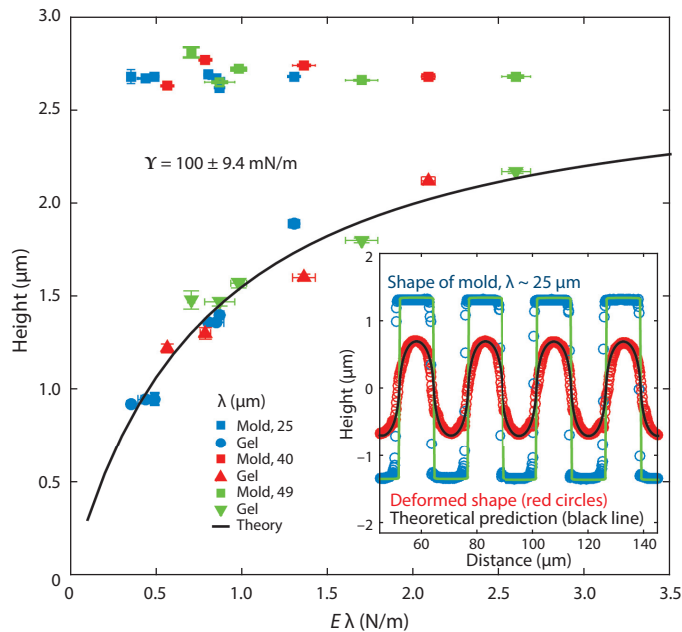


Figure 2

Flattening of a solid surface by surface stress. A gelatin gel with Young's modulus $E = 32.5$ kPa is cured (stress-free) in a silicone mold, then released and allowed to relax under the influence of surface stress. Surface profiles before and after release for different stiffnesses and wavelengths are shown. The x -axis is Young's modulus \times surface wavelength, and the black curve shows the theoretical prediction. The inset shows optical profilometry (theory) measurements of the surface profile of the mold before [blue (green)] and after release [red (black)]. Adapted from Reference 37 with permission.

stress $\sigma_{\text{el}} \sim E\epsilon \sim EA/\lambda$. Thus, flattening is significant when $\sigma_{\gamma} \sim \sigma_{\text{el}}$ or when $\lambda \sim \gamma/E$. In short, elasticity prevents deformation at longer length scales, and surface stress overwhelms elasticity and flattens the surface at smaller scales. Similar arguments show that sharp corners round out to leave a smooth surface with a radius of curvature $\sim \gamma/E$ (36).

In a similar vein, surface stresses also suppress compressional instabilities of soft-solid films. It is well known that confined layers of elastic solids become unstable to buckling, wrinkling or creasing when compressed or swollen (e.g., 38). However the morphology of the surface instability, the critical compression threshold, and the critical defect size for instability nucleation all depend sensitively on the relative size of the layer thickness, H , and elastocapillary length γ/E (e.g., **Figure 3a,b**). For example, when $\gamma/HE \ll 1$, the surface becomes unstable to creases with wavelength $\propto H$ (10, 31, 39). However, when $\gamma/HE \gg 1$, the surface tends to wrinkle instead with wavelength $\gg H$ while the compression needed for the instability to occur increases significantly beyond classical predictions (31, 39–42).

2.3. Surface Stresses Deform Rods

Some of the most dramatic effects of surface stress in solids are seen in objects with slender sections. Surface stresses deform long, thin cylindrical beams of soft hydrogels when they are released from rigid molds (12, 33). Sufficiently thin cylinders develop undulations along their axis, as shown in

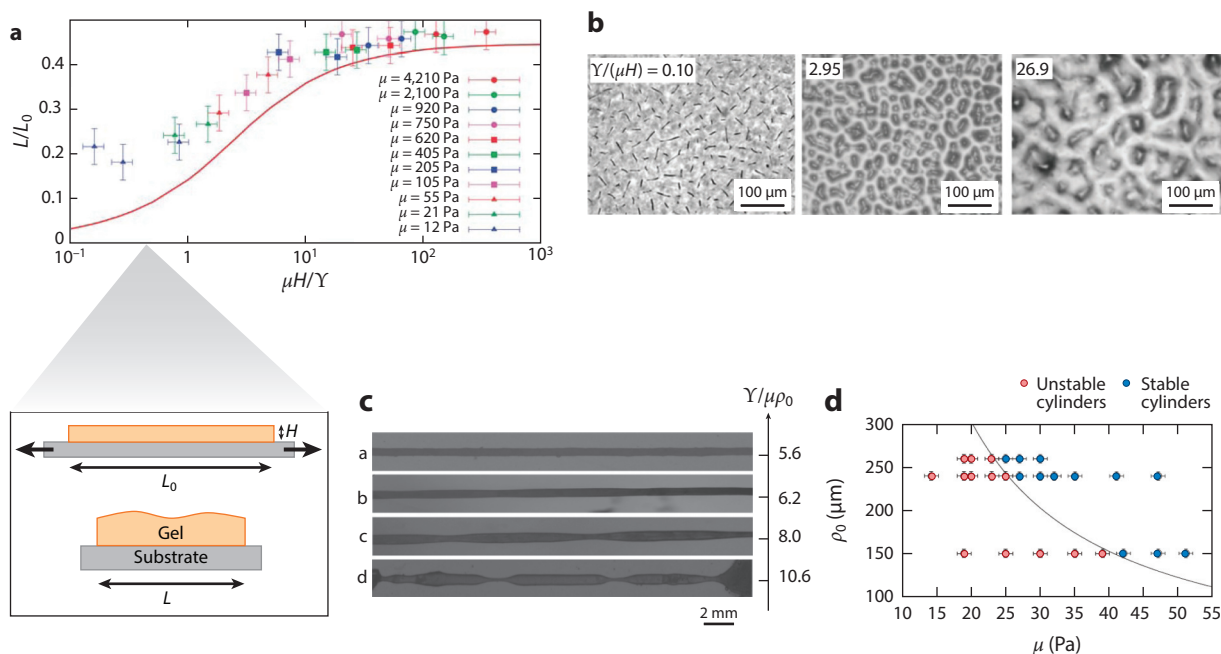


Figure 3

(a) In uniaxial compression of a soft layer (see schematic), the critical compression for instability depends only on the ratio γ/HE ; n.b. soft gels are typically approximately incompressible so their shear moduli $\mu \approx E/3$. Adapted from Reference 31 with permission. (b) Soft silicone layers of varying thickness are swollen by applying an electric field across them. As the ratio γ/HE varies, there is a dramatic shift in the form of the surface instability. Adapted from Reference 39 with permission. (c) Cylinders of soft agar gels are released in toluene and allowed to relax. From top to bottom, the cylinders have μ , reducing from 27 Pa to 12 Pa. (d) The cylinders become unstable (red points) when their diameters ($2\rho_0$) are less than γ/E —this theoretical prediction is given by the curve. Blue points show stable cylinders. Panels c and d adapted from Reference 12 with permission.

Figure 3c (12). This instability is analogous to the famous Rayleigh-Plateau capillary instability (43). In that case, surface tension destabilizes a liquid cylinder of radius R to surface perturbations that have wavelength $\gtrsim O(R)$. In the case of a soft gel, however, this only occurs when the cylinder diameter is less than Υ/E , as shown in **Figure 3c,d**. Additionally, surface stresses round out a slender object's corners, and when it has an asymmetric cross section, the resulting asymmetric surface forces can cause significant bending (33).

2.4. Surface Stresses Stiffen Inclusions and Composites

Surface stresses stabilize spherical fluid inclusions in soft solids. When a soft gel with a dilute concentration of embedded liquid droplets (13) is strained macroscopically, the embedded droplets also deform. However, the extent of deformation depends on the size of the droplets. **Figure 4a** shows three inclusions of different initial sizes subjected to increasing far-field strains. At the same imposed strains, the smaller the inclusion, the more spherical it remains. For a given macroscopic deformation, the droplet strain varies smoothly with its radius (**Figure 4b**). When $\Upsilon/RE \ll 1$, the

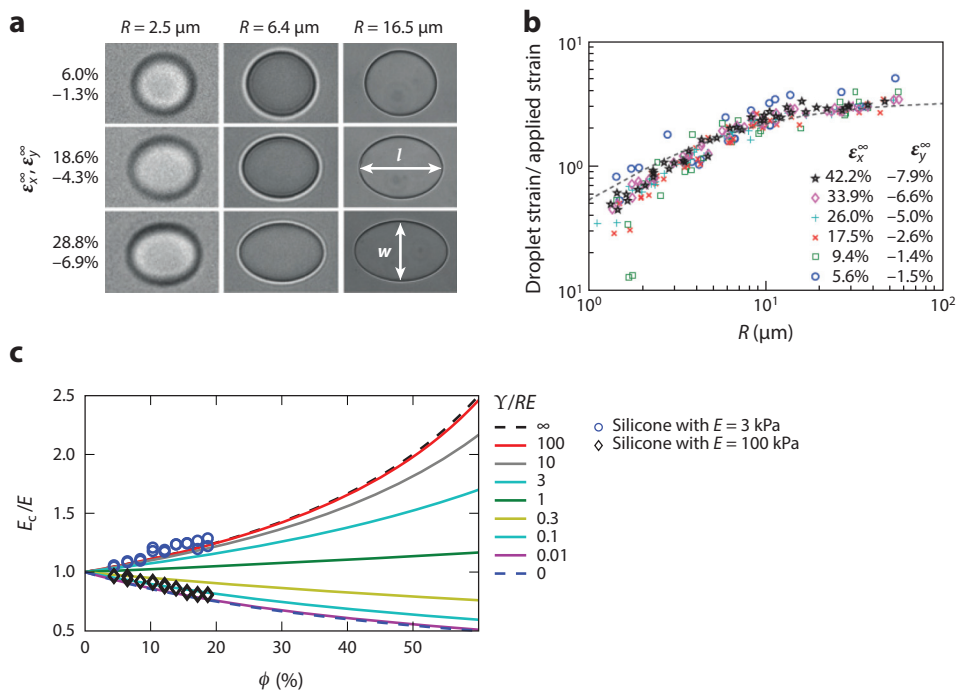


Figure 4

Surface stress affects the shape of small fluid inclusions in a stretched soft solid. Adapted from Reference 13 with permission. (a) Ionic liquid droplets of different initial radii, R , are embedded in a soft silicone sheet and stretched under plane-stress conditions. The applied x, y strains are $\epsilon_x^\infty, \epsilon_y^\infty$, respectively. Smaller droplets stay more spherical. Larger droplets obey classical elasticity theory. (b) Droplet stretch/applied stretch as a function of droplet radius for stretched ionic liquid droplets in a soft silicone gel. Above the elastocapillary length ($\sim 10 \mu\text{m}$), this is approximately constant (i.e., shape is independent of size). Below the elastocapillary length, droplets stretch much less than the surrounding solid. The dashed curve is the theoretical prediction. (c) The stiffness of silicone/glycerol composites as a function of glycerol concentration. Blue circles, silicone with $E = 3$ kPa; black diamonds, silicone with $E = 100$ kPa. In the former, increasing glycerol volume fraction, ϕ , stiffens the composite. Curves: theoretical predictions for composites containing uniformly sized droplets.

droplet shape does not depend on its size, in agreement with Eshelby's classic theory of inclusions in an elastic matrix (44). For $\Upsilon/RE \gg 1$, the droplet shape scales with its size, as surface stresses oppose droplet deformation, contradicting Eshelby's theory.

The stiffening of fluid inclusions by surface tension can have a dramatic impact on the macroscopic behavior of a fluid–solid composite. Intuition and classic composite theory tell us that if you take a solid and fill a volume fraction ϕ of it with fluid-filled holes of radius R , its effective modulus E_c will also decrease as ϕ increases. This works robustly when $\Upsilon/RE \ll 1$. However, the opposite is observed when $\Upsilon/RE \gg 1$. In this case, fluid inclusions actually stiffen the composite solid (**Figure 4c**) (13, 45).

The reason that classic composite mechanics does not work is that it omits Υ , which typically acts to keep inclusions spherical. To address this, much recent work has focused on augmenting composite mechanics to account for surface stresses (e.g., 45–52). The augmented theory shows good agreement with experiments on emulsion (45) and silicone–gel (13) composites when Υ is taken as an isotropic, strain-independent surface stress (**Figure 4b**). The theoretical work again highlights the importance of Υ/E . For example, in incompressible elastic solids containing identical incompressible fluid holes, surface stress becomes important when $R \lesssim 100\Upsilon/E$, causing stiffening relative to classic predictions (51).

A practical simplification for composite calculations is approximating soft inclusions as surface-stress-free, elastic inclusions. For example, in incompressible composites with uniform, isotropic surface stress Υ , liquid inclusions effectively behave like elastic, surface-stress-free inclusions with modulus $E_{\text{eff}}/E = 24/(9 + 10RE/\Upsilon)$ (13, 45, 51). Thus large inclusions have a vanishing effective modulus, small inclusions appear as elastic inclusions with constant stiffness 8/3 times stiffer than the surrounding matrix, and inclusions with $R = 3\Upsilon/2E$ are cloaked with $E_{\text{eff}} = E$. Making this substitution allows us to use the full power of classic composite mechanics to predict the diverse behavior of soft composites.

2.5. Surface Stresses Resist Fracture

Surface stresses also affect the opening of a crack in a soft material (52a). The movement of a crack tip through a solid is governed by the work of fracture Γ , the energy required per unit area of new crack. As this is a material parameter, we can form a second material length scale, an elasto-adhesive length, Γ/E , which characterizes the radius of curvature of a crack tip at propagation (in linear-elastic fracture mechanics) (53). Surface stress then induces a blunting stress on the crack tip $\sigma \sim \Upsilon\kappa \sim \Upsilon E/\Gamma \sim E\epsilon$. Thus a positive surface stress can significantly blunt a crack tip when Υ is comparable to Γ . In this case crack growth is retarded, as pointed out recently (54, 55).

3. ELASTOCAPILLARY PHENOMENA AT CONTACT LINES

So far, we have considered the impact of surface stresses on the mechanics of a single two-phase interface. In this section, we consider the structure of three-phase contact lines when two or more of the phases are soft. First, we consider the wetting of droplets on soft solids. Then, we consider adhesion of rigid particles to soft solids.

3.1. Partial Wetting on Soft Substrates

There are two key results of classic wetting theory. First, Young (56) showed that a droplet's contact angle, θ , on a rigid solid substrate was independent of any far-field boundary conditions (e.g., droplet size or the thickness of a substrate) but varied for different combinations of materials (**Figure 5a**). Minimizing the interfacial energy of the droplet/substrate system, one finds that θ

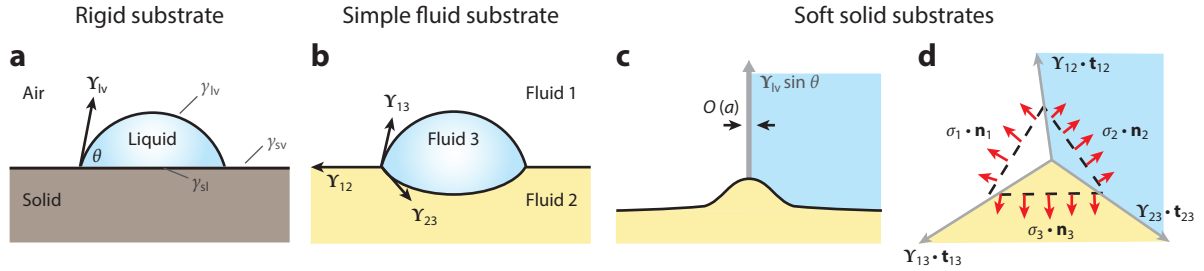


Figure 5

(a) The Young–Dupré law: The contact angle θ is determined by the three surface energies. (b) Neumann’s triangle: The angles at the contact line between three simple fluids are determined by a force balance of the three surface stresses. (c) The nanoscale view of the contact line: The surface stress is spread out over a region of the order of a molecular diameter, a . The resulting pressure pulls the underlying surface up into a ridge. (d) The microscale view of a contact line on a soft solid, showing the forces acting on a small volume (with size $\gg a$) around the contact line.

depends only on the surface energies of the three interfaces, γ_{lv} , γ_{sv} , and γ_{sl} , through the Young–Dupré relation (57):

$$\gamma_{lv} \cos \theta = \gamma_{sv} - \gamma_{sl}. \quad (5)$$

Second, Neumann (58) considered a droplet resting on a liquid substrate with which it is immiscible (**Figure 5b**). At the contact line, the angles between all three interfaces are independent of the far-field boundary conditions and determined by a vector balance of the surface stresses:

$$\mathbf{\Upsilon}_{12} \cdot \mathbf{t}_{12} + \mathbf{\Upsilon}_{13} \cdot \mathbf{t}_{13} + \mathbf{\Upsilon}_{23} \cdot \mathbf{t}_{23} = 0, \quad (6)$$

where the surface stress tensor and the tangent vector of the interface between phases i and j are denoted by $\mathbf{\Upsilon}_{ij}$ and \mathbf{t}_{ij} , respectively. Over the past 100 years, Equations 5 and 6 have served as a basis for understanding the static structure and dynamics of fluids at small scales (20, 59). Recently, however, it has become apparent that wetting on soft solids does not fall simply into either one of these limits.

The complexity arises because a droplet’s surface tension can deform soft solid substrates. For instance, the out-of-plane component of a droplet’s surface tension, $\gamma_{lv} \sin \theta$, pulls up on the surface. To estimate the magnitude of this deformation, let us consider a straight contact line on a semi-infinite, elastic substrate (**Figure 5c**). The line-force, $\gamma_{lv} \sin \theta$, is spread out over a width of the order of the molecular size, a (60–64). The tensile traction applied to the substrate at the contact line can thus be approximated as γ_{lv}/a (65). This produces a strain under the contact line, $\epsilon \approx \gamma_{lv}/Ea$. When this parameter is very small, the substrate is effectively rigid, and the Young–Dupré relation holds (65, 66).

By contrast, when $\gamma_{lv}/E \gtrsim a$, there are significant deformations at the contact line (16, 32, 67–69). In this case, we can determine the contact-line geometry by considering the force balance on a small test volume around the contact line (**Figure 5d**). Equilibrium requires force balance between the bulk and surface stresses:

$$\int_{W_1} \boldsymbol{\sigma}_1 \cdot \mathbf{n}_1 dL + \int_{W_2} \boldsymbol{\sigma}_2 \cdot \mathbf{n}_2 dL + \int_{W_3} \boldsymbol{\sigma}_3 \cdot \mathbf{n}_3 dL + \mathbf{\Upsilon}_{12} \cdot \mathbf{t}_{12} + \mathbf{\Upsilon}_{13} \cdot \mathbf{t}_{13} + \mathbf{\Upsilon}_{23} \cdot \mathbf{t}_{23} = 0. \quad (7)$$

Now shrink the size of the test volume. If the bulk stresses are bounded, or diverge more slowly than $1/r$ (which we expect), their contributions vanish, whereas those from the surface stresses remain finite. In other words, Equation 7 reduces to Neumann’s vector balance, Equation 6, which

requires the three interfaces to meet with fixed orientations (**Figure 5b**) (14, 16, 65, 70–72). Note that this analysis ignores any long-range forces between the interfaces (73, 74).

Thus, microscopic behavior near the contact line depends critically on the parameter Υ_{lv}/Ea . Using the surface tension and molecular dimensions of liquid water, this parameter is of order one for substrates with Young's modulus of 100 MPa. On much stiffer solids, such as structural materials, the Young–Dupré law is recovered. On much softer solids, such as gels, Neumann's triangle describes the contact line geometry. There is a smooth transition between the two limits (15, 65, 71, 75, 76). This phenomenon allowed one of the first techniques for the measurement of the absolute values of solid surface stresses, that is, measuring the angles between the phases at the contact line and the liquid–vapor surface tension (e.g., 20), and using Equation 6 to calculate the solid–vapor and solid–liquid surface stresses.

Although the shape near the contact is universal, the overall shape of the droplet depends on its size (**Figure 6a**). This is related to the fact that the surface stress–dominated regime near the contact line has a width of roughly Υ_{sv}/E , which has been confirmed experimentally (**Figure 6**) (16, 69). For large droplets, $R \gg \Upsilon_{lv}/E$, the wetting ridge is small compared to the droplet size, and the apparent contact angle is unperturbed from its value on a rigid substrate (14). Thus, large droplets behave as if they were on rigid surfaces. In contrast, for small droplets with $R \lesssim \Upsilon_{lv}/E$, the Laplace pressure in the droplet can easily depress the underlying solid surface. In fact, for $R \ll \Upsilon_{lv}/E$, the shape of the droplet is entirely determined by the three interfacial stresses, as it would be for a liquid substrate (**Figure 5b**). There is a smooth transition for the apparent contact angle from the Neumann to the Young–Dupré limits with droplet size, as shown in **Figure 6d**.

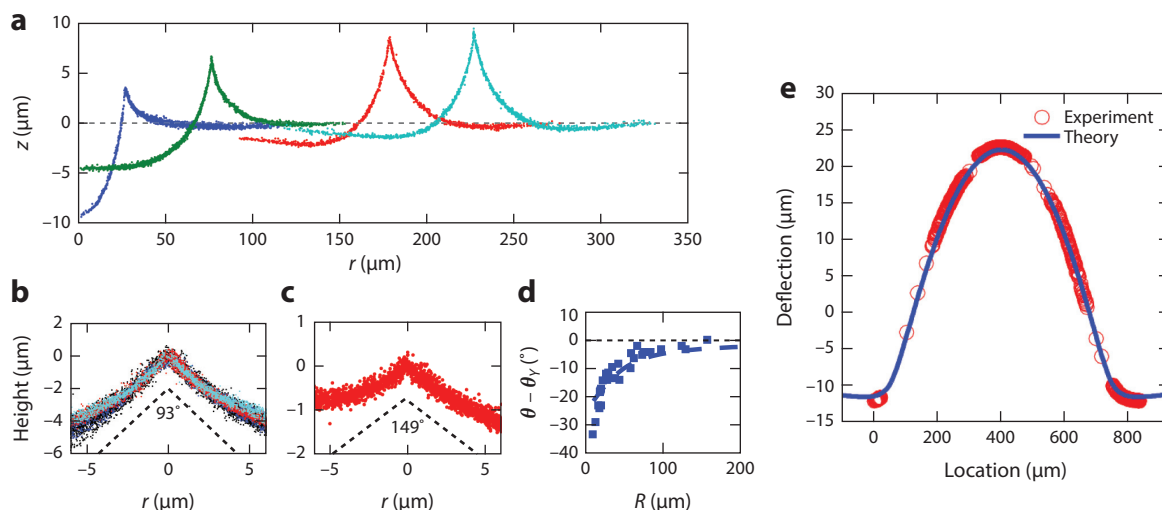


Figure 6

(a–c) Experimental data for droplets on soft, silicone substrates ($E = 3$ kPa). Adapted from Reference 16 with permission. (a) Surface profiles underneath glycerol droplets of different radii. The peaks correspond to the position of the contact line. (b, c) When the surface profiles are aligned (by translation and rotation) at the contact line, the local ridge geometry is always found to be the same for a given liquid/substrate combination. (b, glycerol; c, fluorinated oil). (d) The apparent contact angles θ of glycerol droplets smoothly approach the Young–Dupré limit, θ_Y , as droplet radius increases above the elastocapillary length. The dashed curve shows the linear-elastic theoretical prediction θ . Adapted from Reference 77 with permission. (e) Out-of-plane deflection of a stiff silicone film stretched across an annular disc by the Laplace pressure and surface tension of a water droplet attached to it. The deformed shape can be represented accurately using the theory of plates with in-plane tension. Adapted from Reference 78 with permission.

3.2. Wetting of Slender Objects

When a soft solid has no geometrically imposed length scale, we have seen that liquid surface tension can significantly deform it at scales $\lesssim \Upsilon/E$. However, surface tension can also deform thin rods or sheets made from stiffer materials (c.f. the recent review in Reference 79). In such slender geometries, elastocapillary effects can be significant at length scales much larger than Υ/E . For example, a sessile droplet of characteristic size R can significantly deform a free plate when $R \gtrsim \sqrt{K_b/\gamma_{lv}}$, where $K_b \sim Eb^3$ is the bending stiffness of the plate, and b is the plate thickness. The length scale, $\sqrt{K_b/\gamma_{lv}}$, is also commonly referred to as an elastocapillary length. To avoid confusion with Υ/E , we refer to it as a bendocapillary length, because it describes bending due to capillary forces. Note that $\sqrt{K_b/\gamma_{lv}}$ is not a material parameter, like Υ/E , because it depends on the cross-sectional dimensions of the rod or sheet. Furthermore, bendocapillary phenomena become more pronounced as the system gets larger, in stark contrast to the elastocapillary deformations described in the previous section, where capillary phenomena are more pronounced for smaller droplets. Bendocapillary phenomena are a subject of intense research. Examples include capillary origami and clumping of flexible objects like hair, fibers, and microbeams in microelectromechanical devices by droplets (80–85). An interesting new limit has also recently been identified for the interactions of droplets with extremely bendable sheets (86, 87).

What happens when a sheet carries tension T as well as bending rigidity? For elastic sheets, the Föppl–von Kármán equations predict the response of the sheet to an applied load. By examining the magnitude of the forces due to bending and tension of the sheet, we find a new length scale, $\sqrt{K_b/T}$. Like Υ/E for a thick elastic solid, this length scale captures the intrinsic deformability of a slender elastic object. It does not scale with overall system size but only with the thickness of the sheet. For lateral dimensions much smaller than $\sqrt{K_b/T}$, bending rigidity resists applied forces. On length scales much larger than $\sqrt{K_b/T}$, the sheet’s tension resists applied forces. Consider a small drop placed on the sheet (which exerts a force due to liquid–vapor surface tension at its contact line and a distributed Laplace pressure). If we look very close to the contact line, we will see the influence of the sheet bending. However, if we view the contact line on a sheet on a scale that is intermediate between $\sqrt{K_b/T}$ and the droplet radius, R , the equilibrium configuration should be given by a balance of tensions, a sort of Neumann’s triangle (**Figure 5b**) with the liquid–vapor surface tension balancing the tensions on the wet and dry segments of the sheet.

The tension in an elastic sheet is made up of two contributions, first from the surface stresses on its two sides, $\sim 2\Upsilon$, and second from the bulk elastic stress, $\sim \epsilon Eh$, where ϵ is the tensile strain. Thus for very thin sheets, $b \ll 2\Upsilon/\epsilon E$, the surface stresses dominate, and $T \approx 2\Upsilon$. Then Neumann’s construction implies that significant deformations of the sheet occur when $\gamma_{lv} \gtrsim \Upsilon$. Because typically $\gamma_{lv} \sim \Upsilon$, large deformations are generally expected for sheets in the thin limit.

These simple scaling argument results are supported by recent theory and experiments with droplets placed on thin silicone sheets (78, 88, 89). Thick/stiff plates are undeformed by droplets and thus follow classical wetting behavior, agreeing with the Young–Dupré law. Thin plates deform significantly as the Laplace pressure in the droplet causes the film to bulge out, taking a shape identical to fluid-on-fluid wetting. Note that this transition does not depend on the droplet size, so the experiments can be performed with macroscopic droplets. As an example, **Figure 6e** shows out-of-plane deflection of a silicone film stretched across an annular disc due to the Laplace pressure and surface tension of a water droplet placed under it. The deformed shape can be represented accurately using plate theory (78). At the macroscale, the overall shape at larger length scales resembles a droplet at a fluid–fluid interface: It obeys Neumann’s triangle. Bending is influential only in a small region near the contact edge. The contact angles of the bulging droplets can then be readily measured and used to extract the surface stresses of the sheet (78).

3.3. Adhesion

In adhesion theory, as with wetting, there are two key fundamental results. First, Hertz calculated the force-indentation relationship between two adhesionless, elastic spheres (90). This forms the basis of contact mechanics and works very well for hard materials. Second, Johnson, Kendall & Roberts (JKR) (17) noticed that Hertz's theory breaks down on soft materials—in particular, it cannot explain why there is a significant pull-off force. This is due to adhesion between the surfaces, typically represented by the work of adhesion, W , the energy reduction per unit area of adhered surface (caused by attractive intermolecular forces). For the case of a rigid sphere adhering to a soft substrate, JKR showed that adhesion is important whenever the elasto-adhesion length W/E approaches or exceeds the particle radius, R ; i.e., Hertz \rightarrow JKR when $W/E \gtrsim R$. JKR has been verified experimentally (91) and is widely acknowledged as the standard model for adhesive contact (92). Notably, although it assumes small contact and linear elasticity, it is surprisingly accurate for contact radii, $a \lesssim R/2$ (93).

Recent experiments have shown that JKR theory breaks down on very soft solids (19, 41). For example, load-free glass microspheres were found to indent significantly less into soft silicone gels than would be expected (19). This breakdown occurs because JKR theory neglects the role of surface stress. To see this, consider the process of placing a load-free sphere on a soft substrate. We break the adhesion process into two steps. First, we deform the substrate to its final geometry (**Figure 7a**). Second, we adhere the sphere (**Figure 7b**). JKR theory assumes that in step 1, we only expend energy in elastically deforming the substrate, and this energy comes from the adhesion energy released in step 2. However, as **Figure 7a** illustrates, we have significantly stretched the surface in step 1, meaning that we have also expended energy on surface work.

When does surface stress become important? This can be determined for load-free adhesion by evaluating the work done in stretching the surface, U_γ , and the energy released upon adhesion, U_W . **Figure 7c** shows data for load-free, glass microspheres placed on soft silicone substrates. To a good approximation, the indentation takes the form of a spherical cap in a flat surface. Thus the extra surface area created (by stretching) in the first step is $\sim d^2$ (d is the indentation depth) so $U_\gamma \sim \gamma d^2$. Similarly, the adhesion occurs over the area of the spherical cap, and we find that $U_W \sim WRd$ (R is the sphere radius). Surface stress effects are negligible when $U_\gamma \ll U_W$, or equivalently when $d \ll WR/\gamma$. From classical JKR theory, $d \sim (W^2 R/E^2)^{1/3}$, so the condition for JKR theory to hold becomes $\omega \ll 1$, where $\omega = (W/ER)^{2/3} \gamma/W$ (18, 19, 94–96). This is illustrated in **Figure 7d**, which shows finite-element computations of zero-load, adhesive contact with a rigid spherical indenter (94). When $\omega = 0$, the deformed shape displays the characteristic cusp of JKR theory (17). In the limit of a large elastocapillary number, the surface stress dominates and thus the free surface is horizontal and meets the particle surface at an angle given by the Young–Dupré equation (Equation 5).

In fact, the dimensionless parameter ω completely determines the adhesion behavior, even when a force is applied to the indenter (96). When $\omega \gg 1$, surface stress dominates elasticity (just as in the small droplet on a soft substrate limit). In the limit $\omega \rightarrow 0$, JKR theory predicts that the pull-off force of a rigid spherical indenter from a soft, flat, adhesive substrate is $F_{po} = -3\pi WR/2$. As $\omega \rightarrow \infty$, this pull-off force can be reduced by more than 30% (96). Useful, semianalytical expressions (96) and scaling laws (19, 95, 97) relating force to indentation can be found in recent work, and some results are provided in the **Supplemental Text** (follow the **Supplemental Material** link from the Annual Reviews home page at <http://www.annualreviews.org>).

Surface stress also provides an alternative way to regularize a conceptual difficulty with JKR theory, which predicts an infinite tensile stress at the contact line. This singularity effectively

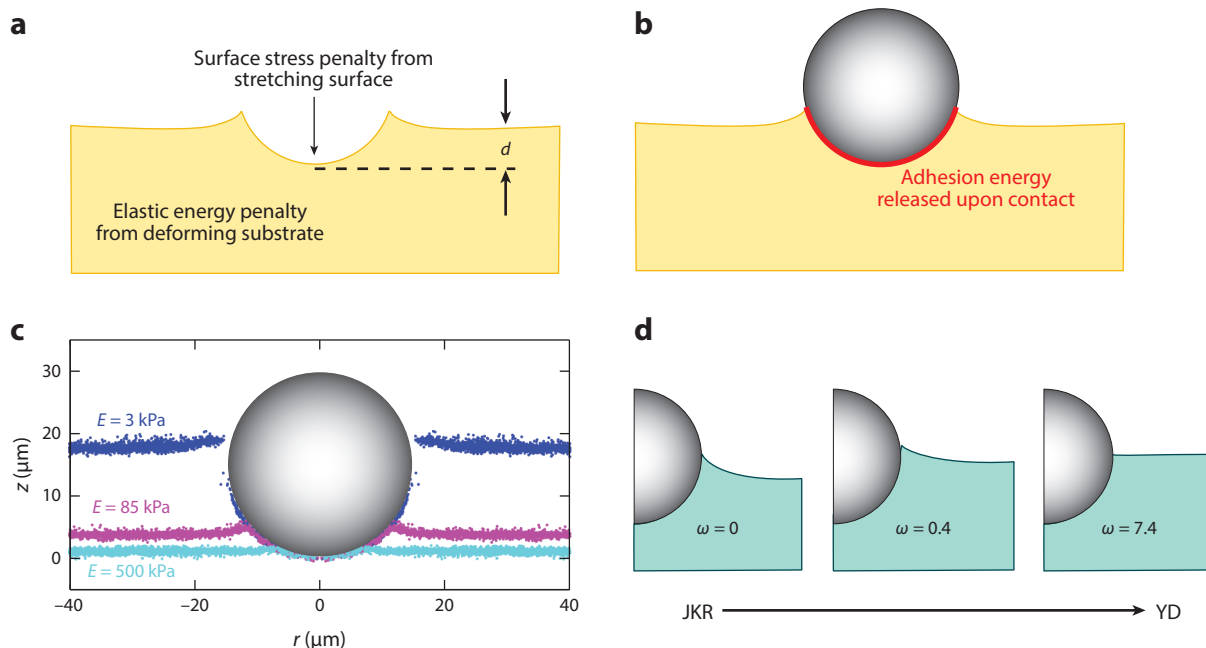


Figure 7

Adhesion of load-free spheres on soft substrates. (a,b) Schematic of the adhesion process of a sphere to a soft substrate. (c) Experimental data for glass microspheres on silicones with three different stiffnesses, measured with confocal microscopy. This panel adapted from Reference 19 with permission. (d) Computed deformed shapes of a substrate in adhesive contact with a rigid sphere under zero external load (94). When the adhesion parameter $\omega = 0$, the deformed shape obeys Johnson–Kendall–Roberts (JKR) theory. When $\omega \gg 1$, the particle behaves as if at a fluid–fluid interface with a contact angle given by the Young–Dupré (YD) equation (Equation 5). This panel adapted from Reference 17 with permission.

reduces JKR contact mechanics to an interface fracture problem (55), which can be regularized by the use of a cohesive zone model (98). Alternatively, recent theoretical work has predicted that for rigid indenters on soft substrates with isotropic surface stresses with $\Upsilon = \gamma$, the soft substrate meets the indenter with a contact angle given by the Young–Dupré law (19, 94, 99). However, some molecular dynamics simulations disagree with this, observing that the contact angle is dependent on parameters including indenter size and substrate stiffness (100). Recent experimental work has demonstrated an alternate mechanism to cut off the elastic stress singularity. Many of the soft solids that demonstrate strong elastocapillary phenomena consist of elastic networks swollen by a solvent. When rigid particles adhere to such a solid, the elastic singularity can be avoided by phase separation of the solvent from the elastic network near the contact line (101, 102).

4. SURFACE STRESS AND SURFACE ENERGY IN SOFT MATERIALS

From a continuum perspective, the interface of two materials is a two-dimensional sheet. Although it has no thickness, the interface can have mechanical properties that drive diverse phenomena. In this section, we review the relationship between two surface properties: the surface energy, γ , and surface stress, Υ . After highlighting key concepts for simple fluids, complex interfaces, and simple solids, we discuss the expected behavior of soft solids like gels.

4.1. Simple Liquid Interfaces

A theoretical understanding of the surface stress of simple liquid interfaces has been complete for some time (103). Simple liquids are isotropic, and their molecules rearrange freely under thermal fluctuations. Thus, the increase in Helmholtz Free Energy (upon changing the surface area A) is simply

$$dF = \gamma dA \Big|_{V,n,T}, \quad (8)$$

with a surface energy, γ , that is independent of fluid deformation or shape. Here V is the volume of liquid, n is the total number of molecules, and T is the temperature. At equilibrium, the change of surface free energy must equal the work done by surface stress upon stretching the surface, $dF = dW$. If we assume that every point on the surface moves from \mathbf{x} to $\mathbf{x} + \Delta\mathbf{x}$, then the work done by the surface stress on an area surrounded by the closed curve C is

$$dW = \oint_C \Delta\mathbf{x} \cdot \boldsymbol{\Upsilon} \cdot \mathbf{b} dl, \quad (9)$$

where \mathbf{b} is the outward normal as in **Figure 1**. Because the interface is an isotropic fluid, the surface stress must be isotropic, $\boldsymbol{\Upsilon} = \Upsilon \mathbf{I}_2$. Then $dW = \Upsilon \oint_C \Delta\mathbf{x} \cdot \mathbf{b} dl = \Upsilon dA$. Comparing this with Equation 8, we conclude that the surface stress and surface energy are numerically equivalent, $\Upsilon = \gamma$.

4.2. Simple Liquid with Insoluble Surfactants

The next level of complexity is a fluid–fluid interface decorated by molecules or particles that are insoluble in the adjoining fluids. Examples include phospholipids, particles, and polymers at interfaces. Because these adsorbed species are confined to the interface, their densities change as the surface is compressed or stretched.

For vanishing concentrations of adsorbed species, the surface stress is isotropic and identical to that of the bare interface, Υ^0 . As the density increases, the surface stress, Υ , decreases. Conventionally, these systems are described by the surface pressure, $\Pi = \Upsilon^0 - \Upsilon$ (104), which is readily measured in a Langmuir trough.

More generally, surface stresses can have isotropic and deviatoric contributions (104, 105):

$$\boldsymbol{\Upsilon} = \text{Tr}(\boldsymbol{\Upsilon}) \mathbf{I}_2 / 3 + \boldsymbol{\Upsilon}^d. \quad (10)$$

The first term is the isotropic tension that opposes increase in surface area. The second, deviatoric part represents in-plane shear forces. This has many possible origins and is quantified by the study of surface rheology (104, 106). For static systems at low concentrations, the surfactant molecules form a dilute, liquid-like layer on the surface that cannot support shear, so $\boldsymbol{\Upsilon}^d = 0$. However, at higher concentrations, surfactants can form solid-like layers on surfaces with $\boldsymbol{\Upsilon}^d \neq 0$. Nonzero $\boldsymbol{\Upsilon}^d$ can also be found in dynamic, fluid-like interfaces at finite rates of shear deformation (105).

4.3. Simple Solid Interfaces

To uncover the connection between surface energy and surface stress for a solid (107), we follow Cahn (108) and distinguish between the reference or Lagrangian configuration R and the current or deformed configuration C . The surface free energy $F = \gamma_R A_R = \gamma_C A_C$ with areas A_R and A_C in the reference and current configurations, respectively, and free energy densities γ_R and γ_C defined per unit area of the reference and current configurations, respectively.

Equating work performed on a system with its change in free energy (similar to the process in Equations 8 and 9), we find

$$\Upsilon = \frac{\partial \gamma_R}{\partial \epsilon^s} \quad (11)$$

(or $\Upsilon_{ij} = \partial \gamma_R / \partial \epsilon_{ij}^s$ in suffix notation), where ϵ^s is the surface strain, which is assumed to be small. This is a 2D version of the familiar connection of stress and free energy used in 3D mechanics. Note that the 2D surface energy density being used is per unit area of the reference configuration. In most cases, it is more convenient to write the surface energy per unit area of the current configuration, γ_C , as that is what is constant in the liquid-like limit. If the strain that connects the two configurations is small, then $A_C = A_R[1 + Tr(\epsilon^s)]$, so $\gamma_C = \gamma_R / [1 + Tr(\epsilon^s)]$. Then, Equation 11 in terms of surface energy density in the deformed configuration becomes

$$\Upsilon = \gamma_C \mathbf{I}_2 + \frac{\partial \gamma_C}{\partial \epsilon^s}. \quad (12)$$

This relationship is known as Shuttleworth's equation (21).

For small, elastic surface strains, we can derive a general form of the surface stress by Taylor-expanding γ_R in terms of ϵ_{ij}^s (here, we use suffix notation with the summation convention). To leading order,

$$\gamma_R = \gamma_0 + B_{ij}\epsilon_{ij}^s + \frac{1}{2}C_{ijkl}\epsilon_{ij}^s\epsilon_{kl}^s. \quad (13)$$

If we also assume that the material is isotropic, then $B_{ij} = \Upsilon_0\delta_{ij}$ and $C_{ijkl} = \lambda^s\delta_{ij}\delta_{kl} + \mu^s(\delta_{ik}\delta_{jl} + \delta_{il}\delta_{jk})$. With these, Equation 11 gives that, at leading order,

$$\Upsilon_{ij} = \Upsilon_0\delta_{ij} + \lambda^s\epsilon_{kk}^s\delta_{ij} + 2\mu^s\epsilon_{ij}^s. \quad (14)$$

This is the general linear-elastic form of the surface stress. λ^s and μ^s are the surface Lamé constants. By analogy with bulk elasticity, μ^s is the surface shear modulus, and $K^s = \lambda^s + 2\mu^s/3$ is the surface bulk modulus or Gibbs elasticity. If the surface Lamé constants are vanishingly small, the magnitude of surface stress is constant and need not equal the surface free energy.

4.4. Soft Solid Interfaces

Now we put forward some simple hypotheses for the form of the surface stress and surface energy of a soft solid. We restrict our attention to polymer gels and elastomers, which have been the focus of experimental studies of elastocapillary phenomena. Gels consist of cross-linked networks of polymer swollen by a solvent, whereas elastomers have no solvent.

In the limiting scenario of the ideal gel, the surface of the elastic network has the same structure and composition as the bulk. Here, as a gel is deformed, solvent can move freely between the surface and bulk. For a dilute gel, the bulk of the surface material is liquid, and thus the surface energy is approximately that of the solvent: $\gamma_C \approx \gamma_l$. Under these conditions, the gel has an isotropic surface stress with a magnitude that is identical to the surface energy (109, 110). This assumption is consistent with many experimental studies on soft hydrogels, as described in earlier sections (see, e.g., 12, 31, 33).

Generally, however, the polymer network is perturbed by the presence of the surface. For example, polymer chains could preferentially adsorb to the surface or the cross-linking density could vary near the surface. Let us consider a simple extension of the ideal gel where a gel with bulk Lamé moduli λ_1, μ_1 has stiffer moduli λ_2, μ_2 within a distance, b , from the surface. Here, b is assumed to be much smaller than other length scales in the problem, so we can subsume the effects of the surface layer into a surface stress term. Assuming the surface zone is still fully permeable to solvent, then there is a constant contribution from the solvent's surface tension, as in the ideal

gel. Then, under certain conditions (e.g., provided b is sufficiently small; see Reference 111), the effective interface condition becomes

$$\Upsilon_{ij} = \gamma \delta_{ij} + \frac{2\mu_2 \lambda_2 b}{\lambda_2 + 2\mu_2} \epsilon_{kk}^s \delta_{ij} + 2\mu_2 b \epsilon_{ij}^s, \quad (15)$$


where ϵ_{ij}^s is the surface strain. This simple model is consistent with the general expression for solid surface stress above (Equation 14). If the moduli of the surface layer are of a similar magnitude to moduli in soft gels and elastomers, and b is no larger than a few tens of nanometers, then we expect the strain-dependent terms to be quite small compared to γ_1 for moderate strains. However, if the moduli of the surface layer are much larger than those in the bulk, the strain-dependent terms become significant. This may be expected when polymer chains, or another component of the system, absorb strongly to the interface.

This, perhaps, is the simplest example one could imagine for nontrivial surface rheology of a gel, i.e., $\Upsilon \neq \gamma \mathbf{I}_2$. It is very likely that the full menagerie of surface rheological behavior such as that seen in complex liquid systems (Section 4.2) can occur on the interfaces of soft solids. Further progress requires systematic measurements of the surface stress in soft solids.

5. ANALYTICAL AND NUMERICAL METHODS

Several methods for analysis of deformation of soft solids that account for surface stress have been developed and used. These include the following:

1. Green's functions for continuum analyses of small-strain elastic deformations that incorporate the boundary condition (Equation 4) described in Section 2.1 (65, 96, 112–115). These are useful for developing analytical and semianalytical solutions, as well as scaling relationships. A key result is that the singularity of the stress and deformation fields at point or line loads on linear-elastic surfaces is reduced significantly by the ability of surface stress to resist deformation. Green's function techniques are closely related to transform methods, which have proven useful in solving elastocapillarity problems. These include Fourier transforms (2D geometries: 32), Hankel transforms (axisymmetric geometries: 14, 72), and Legendre transforms (spherical geometries: 132).
2. General purpose computational (e.g., finite element) methods (30, 33, 116–119). These methods typically represent the role of surface stress in a modular way, say, as a surface finite element, which allows surface stress effects to be combined with nearly any form of bulk mechanical behavior. In the **Supplemental Text**, we describe a two-node surface finite element for use with nonlinear, implicit, static, finite-element simulations for including the influence of surface stress in plane stress/strain and axisymmetric models. We provide a user element file (`usurf_2n_2d_axi.f`) for use with the commercial finite element code *ABAQUS*®, as well as an input file each for 2D (`Rippled.inp`) and axisymmetric (`Hole_axi.inp`) examples.
3. Molecular dynamics and density functional methods. In molecular dynamics methods, continuum properties such as elastic moduli and surface stress emerge automatically in terms of the underlying interparticle potentials. They have been used successfully to study elastocapillary phenomena including contact mechanics (18, 95, 100) and wetting (76, 120). They are best suited to relatively small length scales. An alternative approach is density functional theory. This shares some of the features of molecular simulation in that it is a microscopic calculation based on interparticle potentials. However, the model is solved semianalytically, neglecting fluctuations and representing densities by smooth functions. It is in the spirit of

 Supplemental Material

the classical molecular mechanics methods (103). It has been used, for example, to study the structure near a wetting contact line (15).

Supplemental Material

In the **Supplemental Text**, we provide some further details about the Green's function for 3D and 2D problems, and about a finite element implementation of a surface stress element in the commercial finite element code *ABAQUS*[®] (122).

6. CONCLUSIONS

The research reviewed in this manuscript has established that interfaces in soft solids carry sufficient surface stress to strongly influence and sometimes dominate mechanical phenomena. Collectively, we use the term elastocapillarity to represent these phenomena. In many of these phenomena, the elastocapillary length, Υ/E , defines the characteristic length scale over which surface stress dominates elasticity as the agent resisting (and sometimes driving) deformation. This length scale can be much larger for soft solids such as gels and elastomers than for nonpolymeric solids because the interactions that determine moduli (chain entropic elasticity; 123) are substantially weaker than and disconnected from those that determine surface energy and stress (near-neighbor intermolecular interactions; 20, 124).

In the simplest cases, surface stress is isotropic, homogeneous, and independent of surface strain, and this suffices to explain quantitatively many experiments. In general, surface stresses need not be any of these three. There is also an intimate connection between surface stress Υ and surface free energy γ . This is captured by the Shuttleworth relation, which relates surface stress to how the surface free energy varies with surface strain. It can be used to develop prototypical 2D surface-stress/surface-strain relations. These are analogous to constitutive relations in bulk elasticity that can be derived from a 3D energy density and how it depends on strain. However, the idea of surface stress and more complex surface constitutive behavior need not be limited to those described under thermodynamic equilibrium. We anticipate that soft solid interfaces will exhibit complex rheology, as observed at complex fluid interfaces. Note also that we have assumed in this review that the interface has no bending rigidity (i.e., it cannot support a moment). However, there are many soft interfaces, such as lipid vesicles and cell membranes, where bending rigidity is important (125). Thus a complete description of elastocapillarity may also need to incorporate this possibility (126).

Two-phase systems with a single interface represent the simplest class of problems where the role of surface stresses has been investigated. Phenomena such as the instability and bending of rods, flattening of a structured surface, and stiffening of a solid by liquid inclusions are some of the examples studied so far; there are certainly many others to be studied. For example, the Eshelby theory (which we have seen is strongly modified by surface stress) is widely used beyond composite mechanics, for example, in plasticity (127), fracture mechanics (128) and cell mechanics (129, 130), so surface stress may play a role in these phenomena. In particular, theory suggests that surface stress can strongly attenuate the energy release to a crack tip and thus effectively increase resistance to fracture, but this remains to be tested experimentally. Many soft materials exhibit plasticity, so we expect a whole range of plastocapillary effects, but this area is in its infancy (131, 132). Similarly, much biological material is soft, so there is almost certainly a range of biophysical elastocapillary phenomena to be uncovered (e.g., 133).

The influence of surface stress on three-phase systems has been most studied in the context of wetting (two fluids and one solid), and contact (two solids and one fluid). The departures from classical wetting behavior on soft surfaces have many interesting applications and pose a wide range of questions for future research. One example is the ability to control droplet motion. Droplets spontaneously slide along stiffness gradients toward softer surfaces—this is a process

called droplet durotaxis that has parallels with cellular durotaxis (77). Droplets (77, 134) and even solid objects (135, 136) spontaneously slide toward each other over homogeneous surfaces; this is driven by substrate deformations. Further examples include changes in evaporation, condensation, and droplet-nucleation rates on soft substrates (137–139); increases in the effectiveness of soft colloids as emulsifiers (132, 140); the use of soft surfaces as protection against icing (141); control of the coffee ring effect (142); likely effects on nanobubble and nanodroplet formation on soft surfaces (143); wetting of biological materials; and the potential for adhesion between soft surfaces using nanoparticles (144) and with capillary bridges (145, 146) (a strategy used by many insects; 147). There are many outstanding questions, both theoretical and experimental, still to be tackled. For example, we have known for some time that contact lines typically move at slower speeds on softer substrates. This viscoelastic braking is caused by dissipation in the deforming wetting ridge under a moving contact line (148). It allows the material properties of the substrate to dramatically affect speed, contact angle, and smoothness of contact-line motion (stick-slip or not) (19, 34, 149, 150). Indeed, recent work suggests that contact-line motion can potentially be used as a sensitive measure of substrate rheology (34). A second key area is the measurement of surface stresses: Detailed imaging of the wetting ridge shape is one of the first techniques for measuring absolute values of surface stresses. Although most techniques are based on quasi-static states, vibrational methods for measurement of surface stress are also promising (151). There are also fundamental questions that have arisen from current research. For example, in the case that surface stresses differ in magnitude from their corresponding surface energies, there can be rather counterintuitive effects on substrate strains near the contact line (e.g., 66, 88, 152). Further discussion of the outstanding questions in elastocapillarity can be found in References 35 and 153.

DISCLOSURE STATEMENT

The authors are not aware of any affiliations, memberships, funding, or financial holdings that might be perceived as affecting the objectivity of this review.

ACKNOWLEDGMENTS

We acknowledge vibrant discussions with all of the members of our emerging community, especially those who participated in the Lorentz Center workshop on *Capillarity of Soft Interfaces*. We also acknowledge essential intellectual contributions from long-term collaborators on this topic, including John Wettlaufer and Manoj Chaudhury, and we thank Dominic Vella for helpful discussions on this work. Work by E.R.D. and R.W.S. was supported by the National Science Foundation (CBET-1236086). Work by A.J. and C-Y.H. was supported by the US Department of Energy (DOE), Office of Science, Basic Energy Sciences (BES), Division of Material Sciences and Engineering under Award DE-FG02-07ER46463.

LITERATURE CITED

1. Shepherd RF, Ilievski F, Choi W, Morin SA, Stokes AA, et al. 2011. *PNAS* 108:20400–3
2. Morin SA, Shepherd RF, Kwok SW, Stokes AA, Nemiroski A, Whitesides GM. 2012. *Science* 337:828–32
3. Wood R, Walsh C. 2013. *Sci. Transl. Med.* 5(210):210ed19
4. Suo Z, Ma E, Gleskova H, Wagner S. 1999. *Appl. Phys. Lett.* 74:1177–79
5. Lingley AR, Ali M, Liao Y, Mirjalili R, Klonner M, et al. 2011. *J. Micromech. Microeng.* 21:125014
6. Keplinger C, Sun JY, Foo CC, Rothmund P, Whitesides GM, Suo Z. 2013. *Science* 341:984–87
7. Sun JY, Keplinger C, Whitesides GM, Suo Z. 2014. *Adv. Mater.* 26:7608–14
8. Shin H, Jo S, Mikos AG. 2003. *Biomaterials* 24:4353–64

9. Gordon JE. 1978. *Structures: Or Why Things Don't Fall Down*. Cambridge, MA: Da Capo
10. Chen D, Cai S, Suo Z, Hayward RC. 2012. *Phys. Rev. Lett.* 109:038001
11. Jagota A, Paretkar D, Ghatak A. 2012. *Phys. Rev. E* 85:051602
12. Mora S, Phou T, Fromental JM, Pismen LM, Pomeau Y. 2010. *Phys. Rev. Lett.* 105:214301
13. Style RW, Boltyskiy R, Allen B, Jensen KE, Foote HP, et al. 2015. *Nat. Phys.* 11:82–87
14. Style RW, Dufresne ER. 2012. *Soft Matter* 8:7177
15. Marchand A, Das S, Snoeijer JH, Andreotti B. 2012. *Phys. Rev. Lett.* 109:236101
16. Style RW, Che Y, Wettlaufer JS, Wilen LA, Dufresne ER. 2013. *Phys. Rev. Lett.* 110:066103
17. Johnson K, Kendall K, Roberts A. 1971. *Proc. R. Soc. A* 324:301
18. Carrillo JMY, Dobrynin AV. 2012. *Langmuir* 28:10881–90
19. Style RW, Hyland C, Boltyskiy R, Wettlaufer JS, Dufresne ER. 2013. *Nat. Commun.* 4:2728
20. de Gennes PG, Brochard-Wyart F, Quere D. 2010. *Capillarity and Wetting Phenomena: Drops, Bubbles, Pearls, Waves*. New York: Springer
21. Shuttleworth R. 1950. *Proc. Phys. Soc. A* 63:444
22. Nicolson MM. 1955. *Proc. R. Soc. A* 228:490–510
23. Gurtin ME, Murdoch AI. 1975. *Arch. Rational Mech. Anal.* 57:291–323
24. Gurtin ME, Murdoch AI. 1978. *Int. J. Solid. Struct.* 14:431–40
25. Cammarata R, Sieradzki K. 1994. *Annu. Rev. Mater. Sci.* 24:215–34
26. Spaepen F. 2000. *Acta Mater.* 48:31–42
27. Haiss W. 2001. *Rep. Prog. Phys.* 64:591
28. Sander D. 2003. *Curr. Opin. Solid State Mater. Sci.* 7:51–57
29. Chen T, Chiu MS, Weng CN. 2006. *J. Appl. Phys.* 100:074308
30. Javili A, McBride A, Steinmann P, Reddy B. 2014. *Comp. Mech.* 54:745–62
31. Mora S, Abkarian M, Tabuteau H, Pomeau Y. 2011. *Soft Matter* 7:10612
32. Jerison ER, Xu Y, Wilen LA, Dufresne ER. 2011. *Phys. Rev. Lett.* 106:186103
33. Mora S, Maurini C, Phou T, Fromental JM, Audoly B, Pomeau Y. 2013. *Phys. Rev. Lett.* 111:114301
34. Karpitschka S, Das S, van Gorpum M, Perrin H, Andreotti B, Snoeijer J. 2015. *Nat. Commun.* 6:7891
35. Andreotti B, Baumchen O, Boulogne F, Daniels KE, Dufresne ER, et al. 2016. *Soft Matter* 12:2993–96
36. Gordan OD, Persson BN, Cesa CM, Mayer D, Hoffmann B, et al. 2008. *Langmuir* 24:6636–39
37. Paretkar D, Xu X, Hui CY, Jagota A. 2014. *Soft Matter* 10:4084–90
38. Wang Q, Zhao X. 2014. *J. Appl. Mech.* 81:051004
39. Wang Q, Zhao X. 2013. *Phys. Rev. E* 88:042403
40. Biot MA. 1963. *Appl. Sci. Res. A* 12:168–82
41. Chakrabarti A, Chaudhury MK. 2013. *Langmuir* 29:6926–35
42. Chaudhury MK, Chakrabarti A, Ghatak A. 2015. *Euro. Phys. J. E* 38:1–26
43. Plateau J. 1873. *Statique Expérimentale et Théorique des Liquides Soumis aux Seules Forces Moléculaires*. Vol. 2. Paris: Gauthier-Villars
44. Eshelby JD. 1957. *Proc. R. Soc. Lond. A* 241:376–96
45. Ducloue L, Pitois O, Goyon J, Chateau X, Ovarlez G. 2014. *Soft Matter* 10:5093–98
46. Sharma P, Ganti S. 2004. *J. Appl. Mech.* 71:663–71
47. Yang F. 2004. *J. Appl. Phys.* 95:3516–20
48. Brisard S, Dormieux L, Kondo D. 2010. *Comp. Mater. Sci.* 50:403–10
49. Duan HL, Wang J, Huang ZP, Karihaloo BL. 2005. *Proc. R. Soc. A* 461:3335–53
50. Duan HL, Yi X, Huang ZP, Wang J. 2007. *Mech. Mater.* 39:81–93
51. Style RW, Wettlaufer JS, Dufresne ER. 2015. *Soft Matter* 11:672–79
52. Wang Y, Henann DL. 2016. *Extreme Mech. Lett.* 9:147–57
- 52a. Kundu S, Crosby AJ. 2009. *Soft Matter* 5:3963–68
53. Creton C, Ciccotti M. 2016. *Rep. Prog. Phys.* 79:046601
54. Liu T, Long R, Hui CY. 2014. *Soft Matter* 10:7723–29
55. Hui CY, Liu T, Schwaab ME. 2016. *Extreme Mech. Lett.* 6:31–36
56. Young T. 1805. *Philos. Trans. R. Soc. Lond.* 95:65
57. Dupré A, Dupré P. 1869. *Théorie Mécanique de la Chaleur*. Paris: Gauthier-Villars
58. Neumann F. 1894. *Vorlesungen ber die Theorie der Capillaritt*. Leipzig, Ger.: B.G. Teubner

59. Maxwell JC. 1878. *Encyclopaedia Britannica*, Vol. 5, pp. 56–71. New York: Samuel L. Hall. 9th ed.
60. Shanahan M, de Gennes PG. 1986. *C. R. Acad. Sci. Paris* 302:517
61. Shanahan M. 1987. *J. Phys. D: Appl. Phys.* 20:945–50
62. Rusanov AI. 1975. *Colloid J. USSR* 37:614–22
63. Rusanov AI. 1978. *J. Colloid Interface Sci.* 63:330–45
64. White LR. 2003. *J. Colloid Interface Sci.* 258:82–96
65. Hui CY, Jagota A. 2014. *Proc. R. Soc. A* 470:20140085
66. Marchand A, Das S, Snoeijer JH, Andreotti B. 2012. *Phys. Rev. Lett.* 108:094301
67. Pericet-Cmara R, Best A, Butt HJ, Bonaccorso E. 2008. *Langmuir* 24:10565–68
68. Pericet-Camara R, Auernhammer GK, Koynov K, Lorenzoni S, Raiteri R, Bonaccorso E. 2009. *Soft Matter* 5:3611
69. Park SJ, Weon BM, San Lee J, Lee J, Kim J, Je JH. 2014. *Nat. Commun.* 5:4369
70. Olives J. 2010. *J. Phys. Condens. Matter* 22:085005
71. Lubbers LA, Weijs JH, Botto L, Das S, Andreotti B, Snoeijer JH. 2014. *J. Fluid Mech.* 747:R1
72. Bostwick JB, Shearer M, Daniels KE. 2014. *Soft Matter* 10:7361–69
73. Weijs JH, Andreotti B, Snoeijer JH. 2013. *Soft Matter* 9:8494–503
74. Weijs JH, Snoeijer JH, Andreotti B. 2014. *Phys. Rev. E* 89:042408
75. Leonforte F, Muller M. 2011. *J. Chem. Phys.* 135:214703
76. Cao Z, Dobrynin AV. 2015. *Macromolecules* 48:443–51
77. Style RW, Che Y, Park SJ, Weon BM, Je JH, et al. 2013. *PNAS* 110:12541
78. Nadermann N, Hui CY, Jagota A. 2013. *PNAS* 110:10541–45
79. Roman B, Bico J. 2010. *J. Phys. Condens. Matter* 22:493101
80. Mastrangelo C, Hsu C. 1993. *J. Microelectromech. Syst.* 2:33–43
81. Bico J, Roman B, Moulin L, Boudaoud A. 2004. *Nature* 432:690
82. Kim HY, Mahadevan L. 2006. *J. Fluid Mech.* 548:141–50
83. Py C, Reverdy P, Doppler L, Bico J, Roman B, Baroud CN. 2007. *Phys. Rev. Lett.* 98:156103
84. Duprat C, Protiere S, Beebe AY, Stone HA. 2012. *Nature* 482:510–13
85. Wei Z, Schneider T, Kim J, Kim HY, Aizenberg J, Mahadevan L. 2015. *Proc. R. Soc. A* 471(2175):20140593
86. Huang J, Juskiewicz M, de Jeu WH, Cerda E, Emrick T, et al. 2007. *Science* 317:650–53
87. Vella D, Huang J, Menon N, Russell TP, Davidovitch B. *Phys. Rev. Lett.* 114:014301
88. Hui CY, Jagota A. 2015. *Soft Matter* 11:8960–67
89. Schulman RD, Dalnoki-Veress K. 2015. *Phys. Rev. Lett.* 115:206101
90. Hertz H. 1882. *J. Reine Angew. Math.* 92:156–71
91. Chaudhury MK, Whitesides GM. 1991. *Langmuir* 7:1013–25
92. Shull KR. 2002. *Mater. Sci. Eng. R: Rep.* 36:1–45
93. Lin YY, Chen HY. 2006. *J. Polym. Sci. B* 44:2912–22
94. Xu X, Jagota A, Hui CY. 2014. *Soft Matter* 10:4625–32
95. Cao Z, Dobrynin AV. 2015. *Langmuir* 31:12520–29
96. Hui C-Y, Liu T, Salez T, Raphael E, Jagota A. 2015. *Proc. R. Soc. A* 471(2175):20140727
97. Carrillo JMY, Raphael E, Dobrynin AV. 2010. *Langmuir* 26:12973–79
98. Maugis D. 1992. *J. Colloid Interface Sci.* 150:243–69
99. Karpitschka S, van Wijngaarden L, Snoeijer JH. 2016. *Soft Matter* 12:4463–71
100. Cao Z, Stevens MJ, Dobrynin AV. 2014. *Macromolecules* 47:3203–9
101. Jensen KE, Sarfati R, Style RW, Boltyskiy R, Chakrabarti A, et al. 2015. *PNAS* 112:14490–94
102. Liu Q, Suo Z. 2016. *Extreme Mech. Lett.* 7:27–33
103. Rowlinson JS, Widom B. 2013. *Molecular Theory of Capillarity*. Oxford, UK: Clarendon
104. Fuller GG, Vermant J. 2012. *Annu. Rev. Chem. Biomol. Eng.* 3:519–43
105. Hermans E, Bhamla MS, Kao P, Fuller GG, Vermant J. 2015. *Soft Matter* 11:8048–57
106. Scriven L. 1960. *Chem. Eng. Sci.* 12:98–108
107. Cammarata R. 2008. *Philos. Mag.* 88:927–48
108. Cahn JW. 1980. *Acta Metall.* 28:1333–38
109. Hui CY, Jagota A. 2013. *Langmuir* 29:11310–16

110. Lu W, Suo Z. 2001. *J. Mech. Phys. Solids* 49:1937–50
111. Benveniste Y, Miloh T. 2007. *J. Elastic.* 88:87–111
112. Hajji M. 1978. *J. Appl. Mech.* 45:320–24
113. Dervaux J, Limat L. 2015. *Proc. R. Soc. A* 471(2176):20140813
114. Sneddon IN. 1995. *Fourier Transforms*. New York: Dover
115. Abramovich M, Stegun IA. 1968. *Handbook of Mathematical Functions*. New York: Dover
116. Henann DL, Bertoldi K. 2014. *Soft Matter* 10:709–17
117. Saksono P, Perić D. 2006. *Comp. Mech.* 38:265–81
118. Jagota A, Argento C, Mazur S. 1998. *J. Appl. Phys.* 83:250–59
119. Li S, Fan H. 2015. *Proc. R. Soc. A* 471:20150224
120. Cao Z, Stevens MJ, Dobrynin AV. 2014. *Macromolecules* 47:6515–21
121. Snoeijer JH, Andreotti B. 2008. *Phys. Fluids* 20:057101
122. Simulia. 2015. *Abaqus User Manuals 6.13*. Fremont, CA: Dassault Syst.
123. Rubinstein M, Colby RH. 2003. *Polymer Physics*. Oxford, UK: Oxford Univ. Press
124. Dee GT, Sauer BB. 1998. *Adv. Phys.* 47:161–205
125. Seifert U. 1997. *Adv. Phys.* 46:13–137
126. Helfrich W. 1973. *Z. Naturforsch. C Bio. Sci.* 28:693–703
127. Hutchinson J. 1970. *Proc. R. Soc. A* 319:247–72
128. Rice JR. 1968. *J. Appl. Mech.* 35:379–86
129. Zemel A, Rehfeldt F, Brown AEX, Discher DE, Safran SA. 2010. *Nat. Phys.* 6:468–73
130. Schwarz US, Safran SA. 2013. *Rev. Mod. Phys.* 85:1327–81
131. German G, Bertola V. 2009. *J. Phys.: Condens. Matter* 21:375111
132. Style RW, Isa L, Dufresne ER. 2015. *Soft Matter* 11:7412–19
133. Gonzalez-Rodriguez D, Sart S, Babataheri A, Tareste D, Barakat AI, et al. 2015. *Phys. Rev. Lett.* 115:088102
134. Karpitschka S, Pandey A, Lubbers LA, Weijs JH, Botto L, et al. 2016. *PNAS* 113(27):7403–7
135. Chakrabarti A, Chaudhury MK. 2014. *Langmuir* 30:4684–93
136. Chakrabarti A, Chaudhury MK. 2014. *Langmuir* 31:1911–20
137. Sokuler M, Auernhammer GK, Roth M, Liu C, Bonaccorso E, Butt HJ. 2010. *Langmuir* 26:1544–47
138. Eslami F, Elliott JAW. 2011. *J. Phys. Chem. B* 115:10646–53
139. Lopes MC, Bonaccorso E. 2012. *Soft Matter* 8:7875–81
140. Mehrabian H, Harting J, Snoeijer JH. 2016. *Soft Matter* 12(4):1062–73
141. Petit J, Bonaccorso E. 2014. *Langmuir* 30:1160–68
142. Lopes MC, Bonaccorso E. 2013. *Soft Matter* 9:7942–50
143. Weijs JH, Lohse D. 2013. *Phys. Rev. Lett.* 110:054501
144. Rose S, PrevotEAU A, Elzire P, Hourdet D, Marcellan A, Leibler L. 2014. *Nature* 505:382–85
145. Wexler JS, Heard TM, Stone HA. 2014. *Phys. Rev. Lett.* 112:066102
146. Li K, Cai S. 2014. *Soft Matter* 10:8202–9
147. Labonte D, Federle W. 2015. *Philos. Trans. R. Soc. Lond. B* 370:20140027
148. Carre A, Gastel JC, Shanahan MER. 1996. *Nature* 379:432–34
149. Chen L, Auernhammer GK, Bonaccorso E. 2011. *Soft Matter* 7:9084–89
150. Kajiy T, Daerr A, Narita T, Royon L, Lequeux F, Limat L. 2013. *Soft Matter* 9:454–61
151. Chakrabarti A, Chaudhury MK. 2014. *Extreme Mech. Lett.* 1:47–53
152. Neukirch S, Antkowiak A, Marigo JJ. 2014. *Phys. Rev. E* 89:012401
153. Andreotti B, Snoeijer JH. 2016. *Europhys. Lett.* 113:66001



Contents

My Career as a Theoretical Physicist—So Far <i>J.S. Langer</i>	1
Quantum Hall Effect: Discovery and Application <i>Klaus von Klitzing</i>	13
Arnold Sommerfeld and Condensed Matter Physics <i>Christian Joas and Michael Eckert</i>	31
Ratchet Effects in Active Matter Systems <i>C.J. Olson Reichhardt and C. Reichhardt</i>	51
Sticky-Sphere Clusters <i>Miranda Holmes-Cerfon</i>	77
Elastocapillarity: Surface Tension and the Mechanics of Soft Solids <i>Robert W. Style, Anand Jagota, Chung-Yuen Hui, and Eric R. Dufresne</i>	99
Nonequilibrium Fluctuational Quantum Electrodynamics: Heat Radiation, Heat Transfer, and Force <i>Giuseppe Bimonte, Thorsten Emig, Mehram Kardar, and Matthias Krüger</i>	119
Quantum-Matter Heterostructures <i>H. Boschker and J. Mannhart</i>	145
Extreme Mechanics: Self-Folding Origami <i>Christian D. Santangelo</i>	165
Phase Transitions and Scaling in Systems Far from Equilibrium <i>Uwe C. Täuber</i>	185
Topological Defects in Symmetry-Protected Topological Phases <i>Jeffrey C.Y. Teo and Taylor L. Hughes</i>	211
Intracellular Oscillations and Waves <i>Carsten Beta and Karsten Kruse</i>	239
Glass and Jamming Transitions: From Exact Results to Finite-Dimensional Descriptions <i>Patrick Charbonneau, Jorge Kurchan, Giorgio Parisi, Pierfrancesco Urbani, and Francesco Zamponi</i>	265

Discovery of Weyl Fermion Semimetals and Topological Fermi Arc States	
<i>M. Zaid Hasan, Su-Yang Xu, Ilya Belopolski, and Shin-Ming Huang</i>	289
Monolayer FeSe on SrTiO ₃	
<i>Dennis Huang and Jennifer E. Hoffman</i>	311
Topological Materials: Weyl Semimetals	
<i>Binghai Yan and Claudia Felser</i>	337
Diagonalizing Transfer Matrices and Matrix Product Operators: A Medley of Exact and Computational Methods	
<i>Jutho Haegeman and Frank Verstraete</i>	355
Andreev Reflection in Superfluid ³ He: A Probe for Quantum Turbulence	
<i>D.I. Bradley, A.M. Guénault, R.P. Haley, G.R. Pickett, and V. Tsepelin</i>	407

Errata

An online log of corrections to *Annual Review of Condensed Matter Physics* articles may be found at <http://www.annualreviews.org/errata/conmatphys>